Anomalous mechanical characteristics of Au/Cu nanocomposite processed by Cu electroplating

AUTHOR(S):

Hakamada, Masataka; Yuasa, Motohiro; Mabuchi, Mamoru

Anomalous mechanical characteristics of Au/Cu nanocomposite processed by Cu electroplating

Masataka Hakamada[a,*], Motohiro Yuasa[b] and Mamoru Mabuchi[a]

[a] *Department of Energy Science and Technology, Graduate School of Energy Science, Kyoto University, Yoshidahonmachi, Sakyo-ku, Kyoto 606-8501, Japan*

[b] *Materials Research Institute for Sustainable Development, National Institute of Advanced Industrial Science and Technology, 2266-98 Anagahora, Shimo-shidami, Moriyama-ku, Nagoya 463-8560, Japan*

*Corresponding author. E-mail: hakamada.masataka.3x@kyoto-u.ac.jp

Anomalous mechanical characteristics of Au/Cu nanocomposite processed by Cu electroplating

An Au/Cu nanocomposite is produced by electroplating Cu on a nanoporous Au, and its mechanical characteristics are investigated by hardness tests. The Au/Cu nanocomposite showed a lower hardness and a lower elastic modulus than the nanoporous Au. Furthermore, annealing caused the nanocomposite to harden twice. Large lattice strains in the Au lattice for the nanocomposite were observed by high-resolution transmission electron microscopy. Also, first-principle calculations showed that lattice strains induce the decreased elastic modulus. Therefore, both the inverse mixing behavior and the hardening via annealing are suggested to be related to the large lattice strains.

Keywords: nanocomposite; mechanical properties; lattice strains; transmission electron microscopy (TEM); first-principles calculations

1. Introduction

Nanoporous metals produced by dealloying are sponge-like materials with open-cell network structures [1]. They have attracted much attention for their potential applications as actuators [2], superparamagnetic films [3], fuel cell electrodes [4], hydrogen storage metals [5], biosensors [6] and DNA selectors [7]. Also, nanocomposites fabricated by filling empty pores of a nanoporous metal with other solids are promising materials for electrocatalysts and supercapacitors [8,9]. According to the mixing rule, when pores of a porous metal are filled with reinforcements, its mechanical characteristics such as the strength and the elastic modulus are expected to monotonically increase with increasing the volume of reinforcements. According to this mixing rule, several studies have shown that mechanical strength of nanoporous Au are enhanced by surface deposition [10,11]. However, when pores become small to nanometers, the mechanical characteristics do not necessarily obey to the mixing rule because interfaces strongly affect the mechanical characteristics. If a lot of disorders are

generated at the interfaces, the mechanical characteristics may be reduced by filling pores with reinforcements.

An experiment in the present work reveals that an Au/Cu nanocomposite shows a lower hardness and a lower elastic modulus than a nanoporous Au. An Au/Cu nanocomposite is produced by electroplating Cu on a nanoporous Au, and its mechanical characteristics are investigated by hardness tests. As a result, the hardness and the elastic modulus are reduced by filling pores of the nanoporous Au with Cu. In particular, it is interesting to note that the elastic modulus is reduced because the elastic modulus is usually less sensitive to microstructure. In the present work, microstructure in the Au/Cu nanocomposite is observed by high-resolution transmission electron microscopy. Besides, first-principle calculations are performed to investigate origins of the reduced elastic modulus.

2. Experimental and calculation details

Au (>99.9 mass %) and Ag (>99.9 mass %) ingots were arc-melted together in an Ar atmosphere to prepare a precursor $Au_{0.3}Ag_{0.7}$ ingot. After homogenization at 1173 K for 24 h in an Ar atmosphere and subsequent cold rolling, nanoporous Au with an average ligament size of 20 nm was formed by free corrosion (without any electrochemical potential) of the alloy at 293 K for 72 h in 70 mass % HNO_3. The relative density of the nanoporous Au was approximately 40%. Au/Cu nanocomposites were fabricated by Cu electroplating on nanoporous Au for 20 min. $CuSO_4 \cdot 7H_2O$ (220 g/l) and H_2SO_4 (60 g/l) were used as the electrolyte, with thiourea (0.02 g/l) as an additive. A half part of $0.1 \times 5 \times 10$ mm^3 nanoporous Au film was used as a working electrode that had a Cu wire fitted around its edges to serve as an electrical contact; thus the effective electrodeposited area was 5×5 mm^2. A counter electrode was a Cu plate. The direct current density was 80

mA/cm^2 and the bath temperature was maintained at 293 K. Annealing was performed in air at 473 K for 0.5–2.5 minutes.

Hardness tests were carried out at room temperature with an apparatus equipped with a diamond microvickers tip with face-to-face angle of 136°. Polished cross sections of electrodeposited and non-electrodeposited parts of the same sample were investigated by the hardness tests after epoxy-resin embedding. Pore structures are occasionally changed by polishing. In the present work, polishing was carefully carried out not to change the pore structure as much as possible. The tip was brought into contact with the specimen that was indented at a constant loading rate of 1.324 mN/s. The load was kept constant at 30 mN for 10 seconds, and then the tip was retracted. Hardness was determined by the calibrated area function of Vickers tip. The tests were performed 10 times for each specimen and the average and standard deviation of hardness and elastic modulus were obtained from the load-displacement curves. The hardness tests at the loading rates of 0.378–13.24 mN/s were also carried out on the Au/Cu nanocomposite and the nanoporous Au specimens to investigate the strain-rate sensitivity of the stress and the activation volume.

Microstructures of the specimens were investigated by scanning electron microscopy (SEM) and transmission electron microscopy (TEM). Specimens observed by TEM were thinned using an Ar ion slicer. Energy-dispersive X-ray (EDX) spectrometry analyses were carried out together with SEM observations, where quantification of concentration was conducted by typical ZAF method and peak calibration was conducted by using pure copper. The elemental analyses of seven Au/Cu nanocomposite specimens by SEM-EDX (probed area: 20 × 20 μm^2) showed that the Cu concentrations were 5–38 at.%. The nanocomposite specimens with a Cu concentration of more than 38 at.% were not investigated because Cu began to deposit

on the outer surface. EDX spectrometry analyses were also performed in TEM for Au ligaments using beryllium sample holder. X-ray diffraction (XRD) analyses were conducted on the sample with the analysed area of 5×5 mm^2, which contains sufficient number of grains, using X'Pert Pro by PANalytical, operated under a standard focusing beam configuration with Cu radiation at 45 kV and 40 mA. Scan rate was 0.025 °/s and data acquisition interval was 0.01°.

Calculations for estimating the elastic modulus were performed using the Cambridge Serial Total-Energy Package (CASTEP) [12], which is based on density-functional theory [13,14] in the generalized gradient approximation within the scheme due to Perdew-Burke-Ernzerhof [15]. The ultrasoft pseudopotentials [16] represented in reciprocal space were used and the Kohn-Sham wave functions of valence electrons were expanded to the plane wave basis set and Gaussian smearing with 0.1 eV width. The atomic and electronic relaxation was continued until the Hellman-Feynman force on each atom was less than 0.01 eV/Å.

First-principles tensile tests were performed to investigate effects of the lattice strain on the modulus of longitudinal elasticity, by changing the lattice spacing of (111) plane in the range of ±10%. A supercell used for the first-principle tensile tests consisted of 48 atoms, arranged in form of 12 layers along the [111] direction (Fig.1 (a)). The initial size of the supercell was 6.0×6.0×28.3 $Å^3$. After the lattice spacing of (111) was changed, the atomic position of the supercell was relaxed. In the present work, the modulus of longitudinal elasticity was determined from the gradient of the tensile stress-strain curve obtained by applying strains of 0.05% to the [111] direction from 0% to 0.2%, neglecting the Poisson's ratio. The tensile stress can be given by

$$\sigma = \frac{1}{\Omega(\varepsilon)} \frac{\partial E_{\text{total}}}{\partial \varepsilon} \tag{1}$$

where the E_{total} is the total energy of the supercell, the ε is the tensile strain and $\Omega(\varepsilon)$ is the volume of the supercell [17,18]. The sampling of the Brillouin zone was accomplished by a 5×5×1 Monkhorst-Pack scheme [19]. The cutoff energy for the basis set was 320 eV.

As shown later, both expansion and contraction of lattice spacing were found in the Au/Cu nanocomposite. It was impossible to calculate the modulus of elasticity by the first-principle tensile tests in the state of coexistence of expanded and contracted lattice spacing. Thus, first-principles shear tests were performed to investigate effects of the lattice strain on the modulus of rigidity because it was possible to calculate the modulus of rigidity in the state of coexistence of expanded and contracted lattice spacing. The supercells contained 24 atoms, and consisted of 12 layers. The initial size of the supercell was 2.9×5.0×28.3 Å^3. Fig. 1 (b) shows the normal model where the lattice parameters are not expanded and contracted, and Fig. 1 (c) shows the strained model where the lattice spacing of (111) is expanded and contracted, by shifting one layer of (111) planes in [111] direction. The shifts of the layer was set to 2.5%, 5%, 7.5% and 10% of (111) lattice spacing. The first-principles shear tests were carried out for the $(111)[11\bar{2}]$ slip system. The atomic positions were relaxed only along the slip direction. In the present work, the modulus of rigidity was determined from the gradient of the shear stress-strain curve obtained by applying strains of 0.25% from 0% to 1.0%. The shear stress can be given by

$$\tau = \frac{1}{\Omega(\gamma)} \frac{\partial E_{\text{total}}}{\partial \gamma} \tag{2}$$

3. Results and discussion

TEM images of the Au/Cu nanocomposite are shown in Figs. 2 (a) and (b). Cu was non-

uniformly deposited in nanoporous Au; there were regions where pores were completely filled by Cu electroplating (black areas in Fig. 2 (a)), and other regions where pores remained empty (Fig. 2 (b)). The regions filled by Cu were homogeneously distributed throughout the specimen. Fig. 2 (c) shows an energy-dispersive X-ray spectrometry analysis at an Au ligament in an area containing no Cu deposition, where circular area with the diameter of approximately 50 nm was probed. Although an Au ligament in an area containing no Cu deposition was measured, peaks for Cu were found. This indicates that electroplated Cu atoms incorporated into an Au ligament.

The results of hardness tests for the Au/Cu nanocomposite and the nanoporous Au are shown in Fig. 3. Surprisingly, the hardness of the nanocomposite was lower than that of the nanoporous Au (Figs. 3 (a) and (b)). Low-magnification SEM observations (Fig. 3 (b)) also revealed that no macroscopic cracks were evident and that the indents were sufficiently larger than the typical length scale (= 200–800 nm) of the nonuniformity in the sample. The elastic modulus, as measured by the load-displacement curves, was also lower for the nanocomposite relative to that for the nanoporous Au. The same result was obtained when the maximum load was reduced from 30 to 15 mN, thus indicating that the large changes in the mechanical properties induced by the Cu electroplating were not related to the specimen thickness. Also, the pore size was not changed by the hardness tests.

Seven nanocomposite specimens with different Cu concentrations were subjected to the hardness tests (Figs. 3 (c) and (d)). The sample hardness and elastic modulus significantly decreased with Cu concentration in the low concentration range of less than 5 at.%, but they both increased for the range 5–21 at.%, and then decreased again for greater than 21 at.% Cu. Thus, the mixing rule did not hold in the Au/Cu nanocomposite, and there were not monotonic relationships between the mechanical

characteristics of Au/Cu nanocomposite and the Cu concentration. It should be noted that all the nanocomposite specimens exhibited reduced mechanical characteristics relative to the nanoporous Au. In the present work, the hardness tests were carried out on a part of electrodeposited areas for measuring the mechanical characteristics of the Au/Cu nanocomposite and on another part of non-electrodeposited areas of the same specimen for measuring them of the nanoporous Au. Thus, the hardness tests were performed exactly under the same condition for the Au/Cu nanocomposite and the nanoporous Au, and anomalous mechanical characteristics of the Au/Cu nanocomposite were not because of artifacts.

Variations in hardness as a function of the loading rate are shown in Fig. 4 for the Au/Cu nanocomposite (with Cu concentration of 8.3 at.%) and the nanoporous Au. The strain-rate dependence of the hardness for the Au/Cu nanocompoiste was as large as that for the nanoporous Au. The strain-rate sensitivity can be given by [20]

$$m = \frac{\sqrt{3}kT}{v^*\sigma} = \frac{3\sqrt{3}kT}{v^*H} \tag{3}$$

where m is the strain-rate sensitivity, k is the Boltzmann constant, T is the absolute temperature, σ is the flow stress, H is the hardness (which is generally assumed to be three times the flow stress), and v^* is the activation energy volume. Hence, the activation volume can be given by

$$v^* = \sqrt{3}kT\left(\frac{\partial \ln \dot{\varepsilon}}{\partial \sigma}\right) \tag{4}$$

where $\dot{\varepsilon}$ is the strain rate. The strain-rate sensitivity of stress and the activation volume for the nanocomposite were found to be 0.032 and $133b^3$, respectively, where b is the Burgers vector of Au. The large strain-rate sensitivity suggests that the rate controlling

process for plastic deformation is related to a thermally activated process. The rate-controlling process for plastic deformation in nanoporous Au is generation of dislocations at the surface [21,22]. Therefore, it is likely that the rate-controlling process for plastic deformation in the nanocomposite is generation of dislocations at interfaces. As shown in Fig. 2 (c), Cu atoms were incorporated into Au ligaments. The Cu atoms may hinder movement of dislocation glide, resulting in solute hardening. If the rate controlling process is related to the solute hardening, the strain-rate sensitivity of the Au/Cu nanocompoiste will be different from that of the nanoporous Au. However, the strain-rate sensitivity of the former was almost the same as that of the latter. Therefore, it is suggested that the solute hardening was minor.

Effects of annealing at 473 K on mechanical characteristics are shown in Fig. 5. The hardness increased with the annealing time up to 2.5 min and the elastic modulus increased with the annealing time up to 2.5 min; as a result, the hardness increased by 100% and the elastic modulus increased by 150%. The enhanced hardness and elastic modulus by annealing cannot be due to pore growth. Annealing-induced hardening in a nanocrystalline metal [23] was related to the mobile dislocation density. However, this is unlikely to explain the nanocomposite annealing results observed, since not only enhanced hardness, but also the enhanced elastic modulus was found. Surface oxidation of Cu may be responsible for the enhanced hardness by annealing. To check this, the hardness of nanoporous Cu was investigated before and after heating at 473 K for 2.5 min. As a result, the hardness was 17 MPa before and 16 MPa after annealing, respectively. This indicates that surface oxidation of Cu was not responsible for the enhanced hardness by annealing. Also, diffusion length of Cu in Au (= $(2Dt)^{1/2}$), where D and t are diffusion coefficient of Cu in Au and annealing time respectively, is estimated to be 5.3×10^{-13} m under the condition of annealing temperature of 473 K

and annealing time of 2.5 min and much shorter than the typical length scale of the nanoporous Au. This excludes the possibility of solid solution strengthening during the annealing.

High-resolution TEM images of the nanocomposite before and after annealing are shown in Figs. 6 (a) and (b). Prior to annealing (Fig. 6 (a)), the nanocomposite lattice spacing varied significantly—from 0.255 nm at the left lower point to 0.234 nm at the left upper point, and 0.212 nm at the right upper point. The associated lattice strains are estimated up to be about 10%, assuming that the normal lattice spacing of 0.235 nm is for Au (111) (it was difficult to accurately identify the observed crystal plane from the diffraction pattern). In Fig. 6 (b), the lattice spacing for the annealed nanocomposite was uniformly 0.233 and 0.234 nm, thus large lattice strains were not present. X-ray diffraction profiles of specimens before and after Cu electroplating are shown in Fig. 6 (c). FWHM of the 220 peak of the specimen after Cu electroplating was 0.56°, which is larger by 0.05° than that (= 0.51°) of the specimen before Cu electroplating. This fact also suggests that the Cu electroplating caused lattice disorder in the nanocomposite.

Strains at the interface in nanocomposites are often generated due to a difference in atomic size, resulting in a dependence of chemical composition of their mechanical characteristics [10,24]. However, as shown in Figs. 3 (c) and (d), there were not monotonic relationships between the mechanical characteristics of Au/Cu nanocomposite and the Cu concentration. Besides, lattice strains in the annealed nanocomposite were very low. Hence, the large lattice strains in the unannealed nanocomposite are not due to the difference in Au and Cu atomic sizes.

The present softening in the Au/Cu nanocomposites is different from the previous studies on surface-modified core-shell nanoporous Au [10,11] reporting

hardening by the surface coverage of the ligaments by the second phase such as Al_2O_3 [10] and Ni [11]. This may be related to the difference in the energy of surface deposition technique. As shown in Fig. 2(c), Cu atoms were present even in the Au ligaments. During electroplating, Cu ions have energies corresponding to several tens of thousands K [25]. Fukai et al. [26] showed that electroplating has an impact as intensive as high-pressure and high-temperature processes. Electroplating is one of processes those are beyond equilibrium. Therefore, it is possible that, during the electroplating, high-energy Cu ions accelerated by the imposed electric field collides with the Au nanoligaments and that reduced Cu atoms are embedded in the crystal lattice of Au, resulting in consequent heavy lattice distortion of crystal lattice of Au.

Since plastic deformation of the Au/Cu nanocomposite derives from dislocations emitted at the interfaces, it follows that large strains at the interfaces generate dislocations; thus the Cu electroplating causes a decrease in hardness that is subsequently recovered by annealing of the lattice strains. However, a decrease in elastic modulus is unlikely to be caused by lattice strains at the interfaces, but instead by lattice strains of internal grains. A metallic glass exhibits a lower elastic modulus than a metallic crystal [27]. This fact supports that the reduced elastic modulus for the Au/Cu nanocomposite is related to the lattice strains of internal grains.

The charge density distribution between first neighbour atoms are responsible for the bond strength of the two atoms. In particular, the charge density at the bond critical point (BCP), which is a saddle point with two negative curvatures and one positive curvatures, midway between each pair of first neighbour atoms is an important factor for the elastic modulus [28]. The charge density at BCP may sensitively change by lattice expansion and contraction because of the flexibility of metallic bond. Because the charge density at the BCP decreases with increasing bond length, expansion of the

lattice spacing by the Cu electroplating may be responsible for the reduced elastic modulus. Hence, it is worthwhile to investigate variations in elastic modulus and charge density at the BCP with the lattice strain. In the present work, variations in modulus of longitudinal elasticity and charge density at the BCP with increasing and decreasing lattice spacing of (111) plane in Au were investigated by the first-principle tensile tests. The results are shown in Fig. 7. It can be seen that the modulus of longitudinal elasticity decreases with increasing the lattice spacing [29,30]. As shown in Fig. 3 (d), the elastic modulus was decreased by approximately 80% in the case of the Cu concentration of 5 at.%. The result in Fig. 7 shows that the large decrease in elastic modulus can be obtained by an increase in lattice spacing by 8.3%. The higher modulus of longitudinal elasticity than experimentally derived ones (~ 80 GPa) of Au may be attributed to neglecting the Poisson's ratio. When the lattice spacing is increased, the charge density at the BCP is decreased (Fig. 7 (b)). Therefore, it is suggested that a reduction in elastic modulus with increased lattice spacing is related to a reduced charge density at the BCP in Au lattices.

The elastic modulus in Fig. 7 was calculated assuming that all lengths of (111) lattice spacing were expanded (or contracted). However, as shown in Fig. 6 (a), both expansion and contraction of lattice spacing were found in the nanocomposite. Thus, the first-principle shear tests were carried out with the cell where both expansion and contraction of (111) lattice spacing coexisted. The variation in modulus of rigidity with the lattice strain is shown in Fig. 8. It is noted that the modulus of rigidity decreases with the lattice strain in the state where both expansion and contraction of (111) lattice spacing are present, for example, the modulus of rigidity decreases by 43.7% in the case of the lattice strain of 10%. Therefore, it is suggested that the lower elastic modulus of the nanocomposite is due to the lattice strain.

4. Conclusions

The present work revealed that the Au/Cu nanocomposite showed a lower hardness and a lower elastic modulus than the nanoporous Au. Furthermore, the Au/Cu nanocomposite unexpectedly hardened by annealing. Large lattice strains in the Au lattice for the nanocomposite were observed by high-resolution transmission electron microscopy. Therefore, both the inverse mixing behavior and the hardening via annealing are suggested to be related to the large lattice strains. The first-principle calculations supported that lattice strains induce the decreased elastic modulus. However, there is much room for study on the present anomalous mechanical properties of Au/Cu nanocomposite; for example, the effects of Cu concentration, pore size of nanoporous Au, annealing temperature and atmosphere on the hardening via annealing are to be investigated for further clarification of operative mechanism therein.

Acknowledgments

M. H. is grateful for financial support from JSPS Grant-in-Aid for Young Scientists (B) 24760572 for preparation of nanoporous metals. M. M. is grateful for financial support from JSPS Grant-in-Aid for Scientific Research (B) 23360305 for TEM observation. The authors thank Prof. T. Yao (Kyoto Univ.) and Prof. T. Yabutsuka (Kyoto Univ.) for their assistance with SEM observation. Thanks are due to Prof. T. Hirato (Kyoto Univ.) for XRD measurement. The authors also thank Dr. Y. Chino (National Institute of Advanced Industrial Science and Technology (AIST)) for preparation of starting alloys.

References

[1] J. Erlebacher, M. J. Aziz, A. Karma, N. Dimitrov and K. Sieradzki, Nature 410 (2001) p.450.

[2] J. Biener, A. Wittstock, L. A. Zepeda-Ruiz, M. M. Biener, V. Zielasek, D. Kramer, R. N. Viswanath, J. Weissmüller, M. Bäumer and A. V. Hamza, Nat. Mater. 8 (2009) p.47.

[3] M. Hakamada, M. Takahashi, T. Furukawa and M. Mabuchi, Appl. Phys. Lett. 94 (2009) p.153105.

[4] J. Snyder, T. Fujita, M. W. Chen and J. Erlebacher, Nat. Mater. 9, (2010) p.904.

[5] M. Hakamada, H. Nakano, T. Furukawa, M. Takahashi and M. Mabuchi, J. Phys. Chem. C 114 (2010) p.868.

[6] K. Hu, D. Lan, X. Li and S. Zhang, Anal. Chem. 80 (2008) p.9124.

[7] S. M. Iqbal, D. Akin and R. Bashir, Nat. Nanotech. 2 (2007) p.243.

[8] Y. Ding, M. Chen and J. Erlebacher, J. Am. Soc. Chem. 126 (2004) p.6876.

[9] X. Lang, A. Hirata, T. Fujita and M. Chen, Nat. Nanotech. 20 (2011) p.232.

[10] M. M. Biener, J. Biener, A. Wichmann, A. Wittstock, T. F. Bäumann, M. Bäumer and A. V. Hamza, Nano Lett. 11 (2011) p.3085.

[11] N. Abdolrahim, D. F. Bahr, B. Revard, C. Reilly, J. Ye, T. J. Balk and H. M. Zbib, Philos. Mag. 93 (2013) p.736.

[12] M. C. Payne, M. P. Teter, D. C. Allan, T. A. Arias and J. D. Joannopoulos, Rev. Mod. Phys. 64 (1992) p.1045.

[13] P. Hohenberg and W. Kohn, Phys. Rev. B136 (1964) p.864.

[14] W. Kohn and L. Sham, Phys. Rev. A140 (1965) p.1133.

[15] J. P. Perdew, K. Burke and M. Ernzerhof, Phys. Rev. Lett. 77 (1996) p.3865.

[16] D. Vanderbilt, Phys. Rev. B 14 (1990) p.7892.

[17] O. H. Nielsen and R. M. Martin, Phys. Rev. B 32 (1985) p.3780.

[18] O. H. Nielsen and R. M. Martin, Phys. Rev. B 32 (1985) p.3792.

[19] H. J. Monkhorst and J. D. Pack, Phys. Rev. B 13 (1976) p.5188.

[20] L. Lu, R. Schwaiger, Z. W. Shan, M. Dao, K. Lu and S. Suresh, Acta Mater. 53 (2005) p.2169.

[21] J. Diao, K. Gall, M. L. Dunn and J. A. Zimmerman, Acta Mater. 54 (2006) p.643.

[22] L. Zuo and A. H. W. Ngan, Philos. Mag. Lett. 86 (2006) p.355.

[23] X. Huang, N. Hansen and N. Tsuji, Science 312 (2006) p.249.

[24] X. W. Liu, J. Hu and B. C. Pan, Physica E 40 (2008) p.3042.

[25] S. Yoshida, *Hakumaku*, Baifukan, Tokyo, 1990 (in Japanese).

[26] Y. Fukai, J. Alloy. Compd. 356–357 (2003) p.263.

[27] T. Zhang and A. Inoue, Mater. Trans. 43 (2002) p.708.

[28] M. E. Eberhart, Acta Mater. 44 (1996) p.2495.

[29] A. Landa, J. Klepeis, P. Söderlind, I. Naumov, O. Velikokhatnyi, L. Vitos and A. Ruban, J. Phys. Chem. Solids 67 (2006) p.2056.

[30] P. Söderlind, J. A. Moriarty and J. M. Wills, Phys. Rev. B 53 (1996) p.14063.

Figure captions

Figure 1. Top and side views of (a) model used for the first-principles tensile tests, (b) normal model used for the first-principles shear tests and (c) strained model used for the first-principles shear tests containing locally shifted (111) layer. The white dashed line in (a) indicates the bond where the charge density at the bond critical point is estimated (Fig. 7 (b)).

Figure 2. (a) TEM image of an Au/Cu nanocomposite. Pores are completely filled by Cu deposition in the black areas, but pores are empty in other areas. Scale bar: 200 nm. (b) Enlarged TEM image of the white square in Fig. 2(a). Pores are not filled by Cu deposition in the white areas. (c) Energy-dispersive X-ray spectrometry analysis at an Au ligament in an area containing no Cu deposition. The analysis reveals that electroplated Cu atoms have incorporated into an Au ligament.

Figure 3. (a) Load-displacement curves for the Au/Cu nanocomposite (red) and the nanoporous Au (black). The hardness and elastic modulus of the nanocomposite are lower than those of the nanoporous Au. (b) SEM images of an indent of the nanocomposite (right) and the nanoporous Au (left) specimen surfaces after the hardness tests. (c) Variation of the hardness as a function of the Cu concentration. (d) Variation of the elastic modulus as a function of the Cu concentration. All the nanocomposite specimens show reduced mechanical characteristics compared with the nanoporous Au specimen. Cu concentrations were measured by SEM-EDX with rectangular probed area of 20 × 20 μm^2. Seven or more areas were analysed and standard deviations for Cu concentration are shown as error bars (some standard deviations are so small that error bar cannot be seen).

Figure 4. Variation of the hardness as a function of the loading rate for the Au/Cu nanocomposite (red) and the nanoporous Au (black). The hardness tests are performed at the loading rates of 0.378–13.24 mN/s. Cu concentration for the Au/Cu composite was 8.3 at.% (analysed with SEM-EDX).

Figure 5. Effects of annealing at 473 K on mechanical characteristics and pore growth. (a) Variation of the hardness as a function of the annealing time for the Au/Cu nanocomposite. (b) Variation of the elastic modulus as a function of the annealing time for the Au/Cu nanocomposite. Note that the hardness and elastic modulus both

increased by annealing for a few minutes. Cu concentration for the Au/Cu composite was 8.3 at.% (analysed with SEM-EDX).

Figure 6. (a) High-resolution TEM image of the Au/Cu nanocomposite before annealing. (b) High-resolution TEM image of the Au/Cu nanocomposite after annealing at 473 K for 2.5 minutes. (c) XRD profiles around Au 220 peaks of the nanoporous Au and the Au/Cu nanocomposite. Cu concentration for the Au/Cu composite was 8.3 at.% (analysed with SEM-EDX).

Figure 7. (a) Variation in modulus of longitudinal elasticity estimated by first-principles tensile tests with change in (111) lattice spacing in Au. (b) Variation in charge density at the bond critical point (Fig. 1 (a)) with change in (111) lattice spacing in Au.

Figure 8. Variation in modulus of rigidity estimated by first-principles shear tests with local change in (111) lattice spacing in Au.

Figure 1

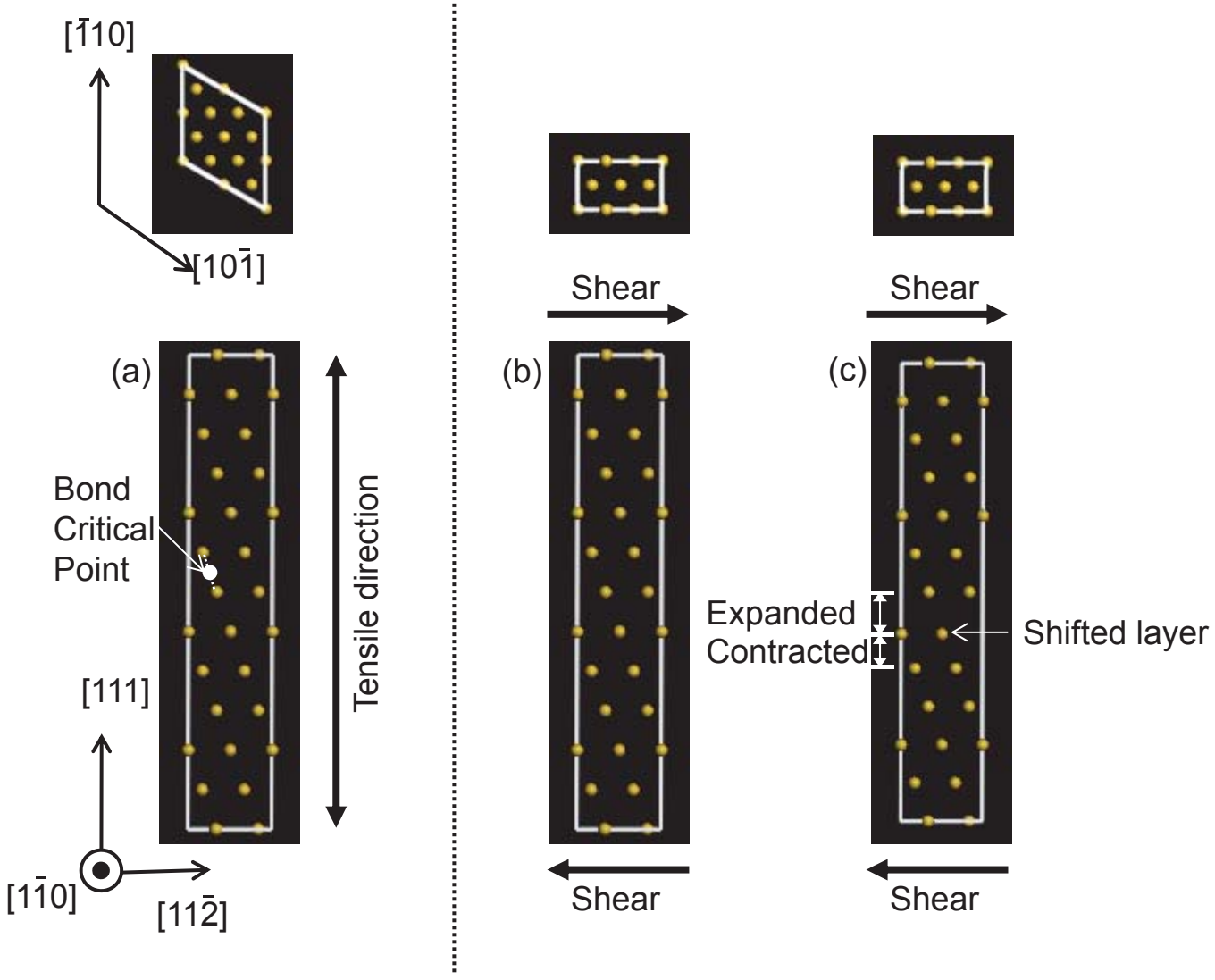

Figure 2

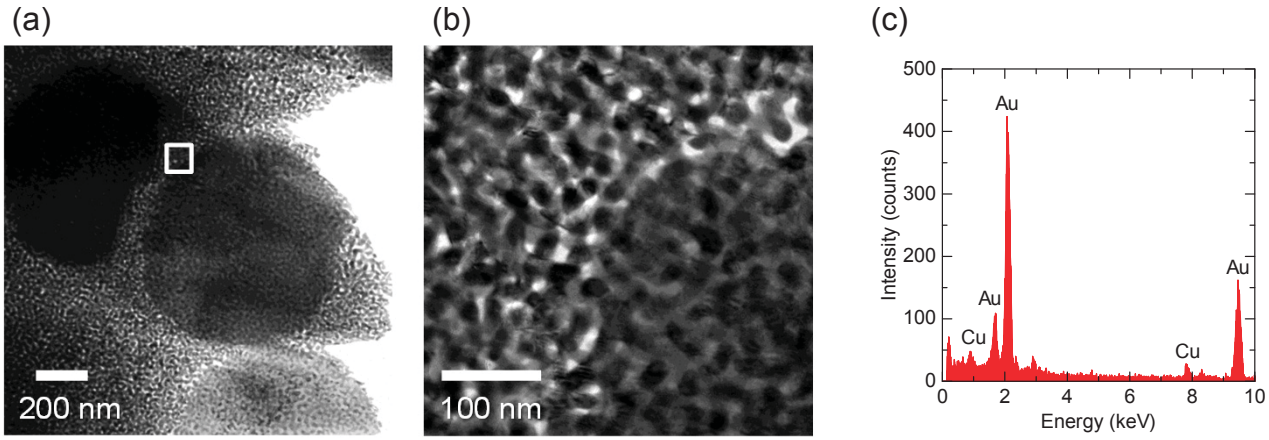

Figure 3

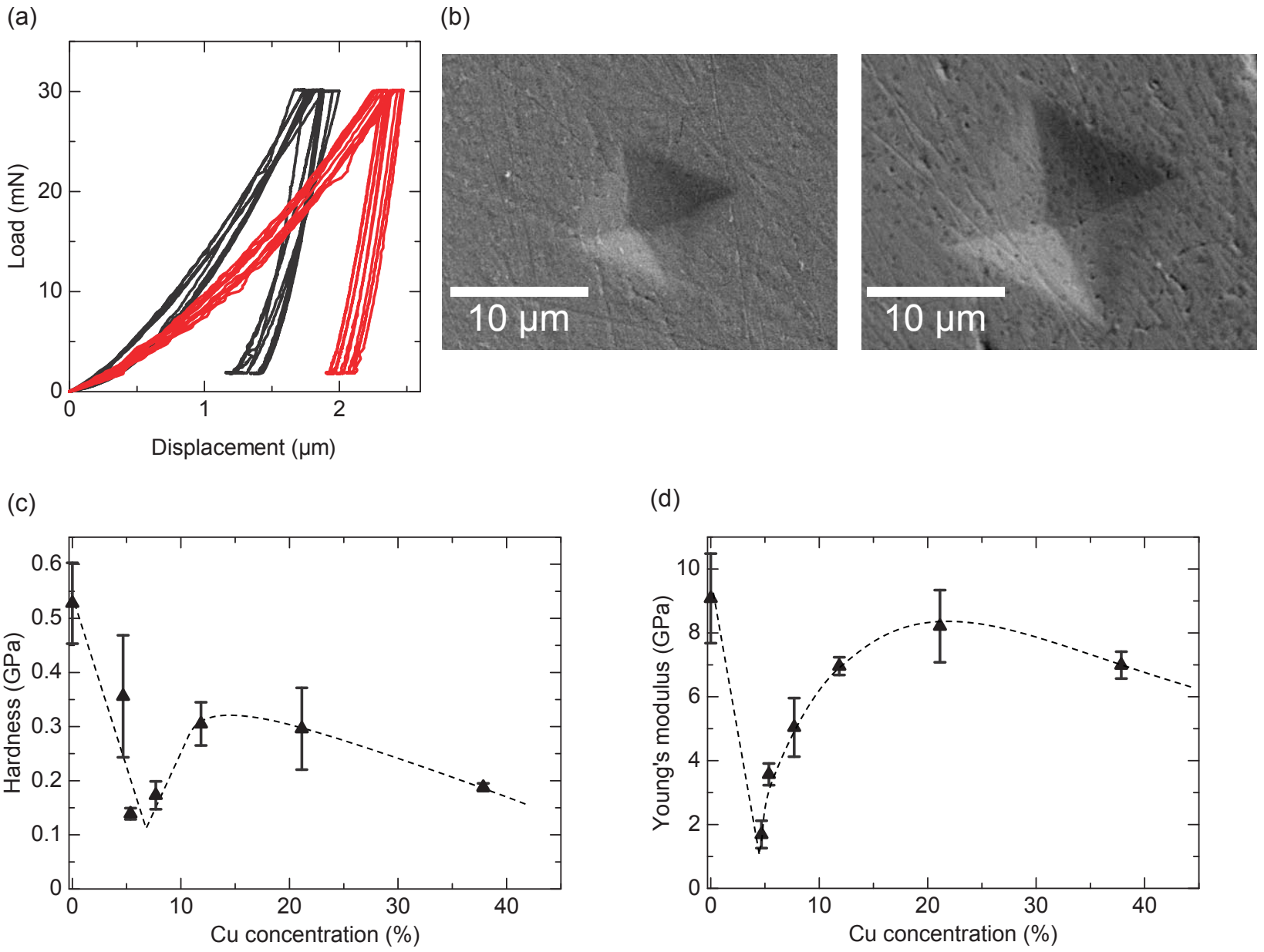

Figure 4

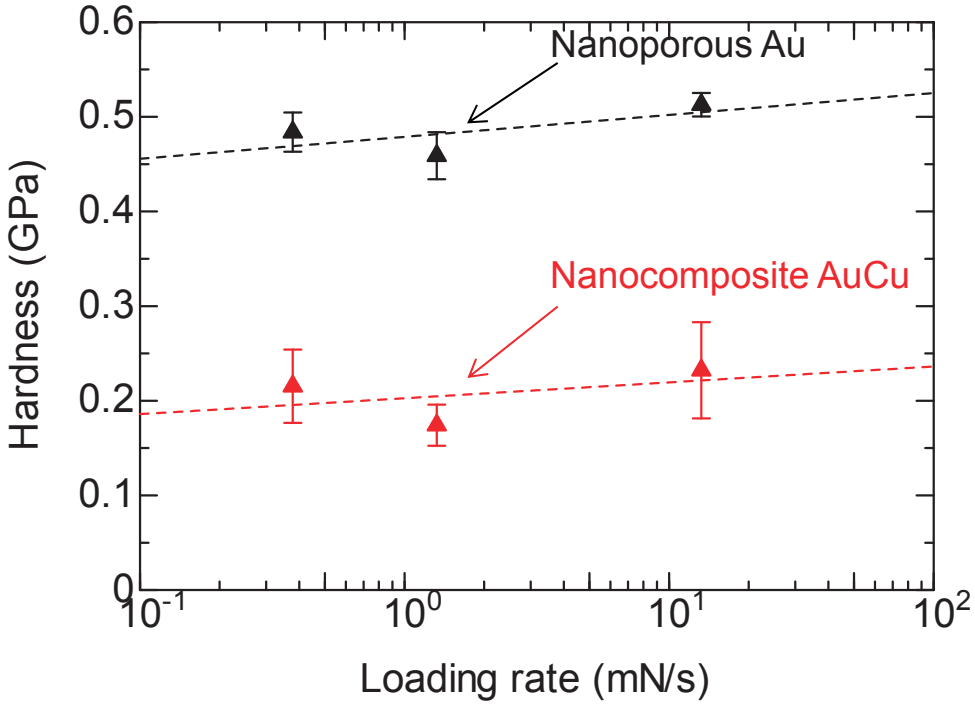

Figure 5

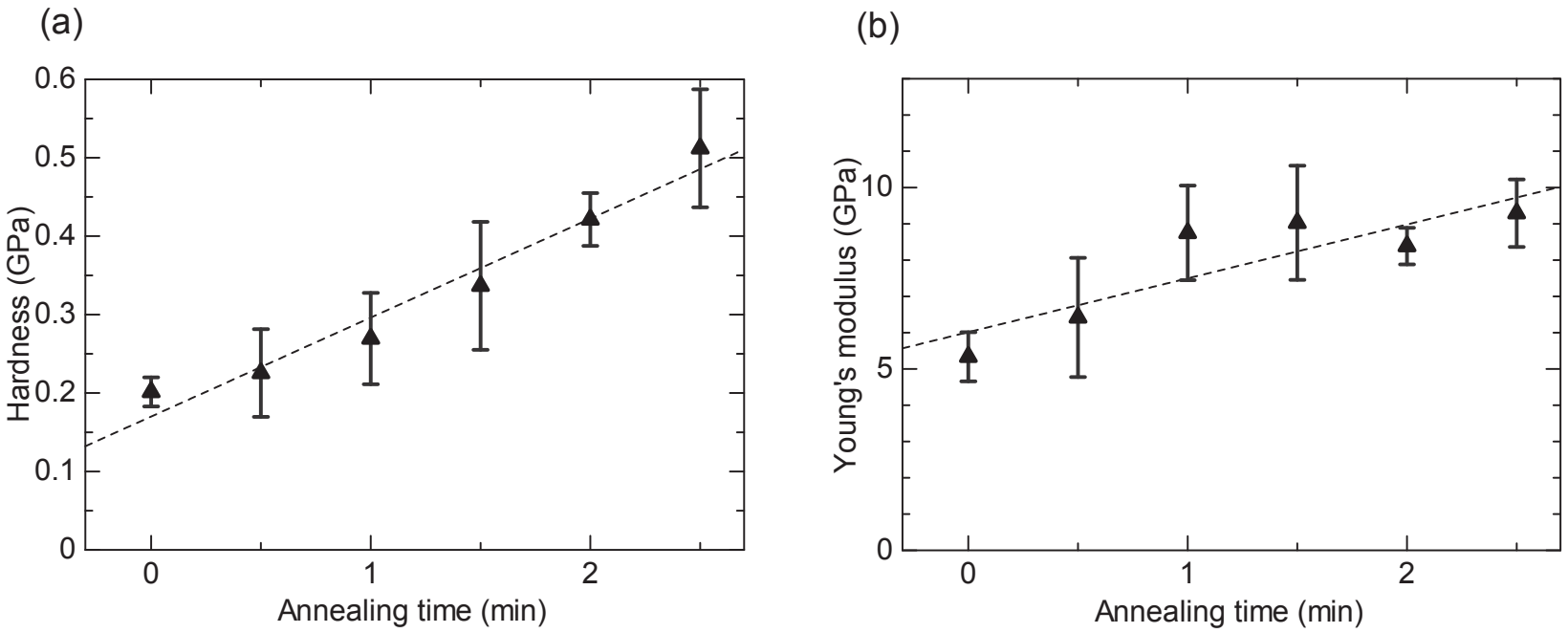

Figure 6

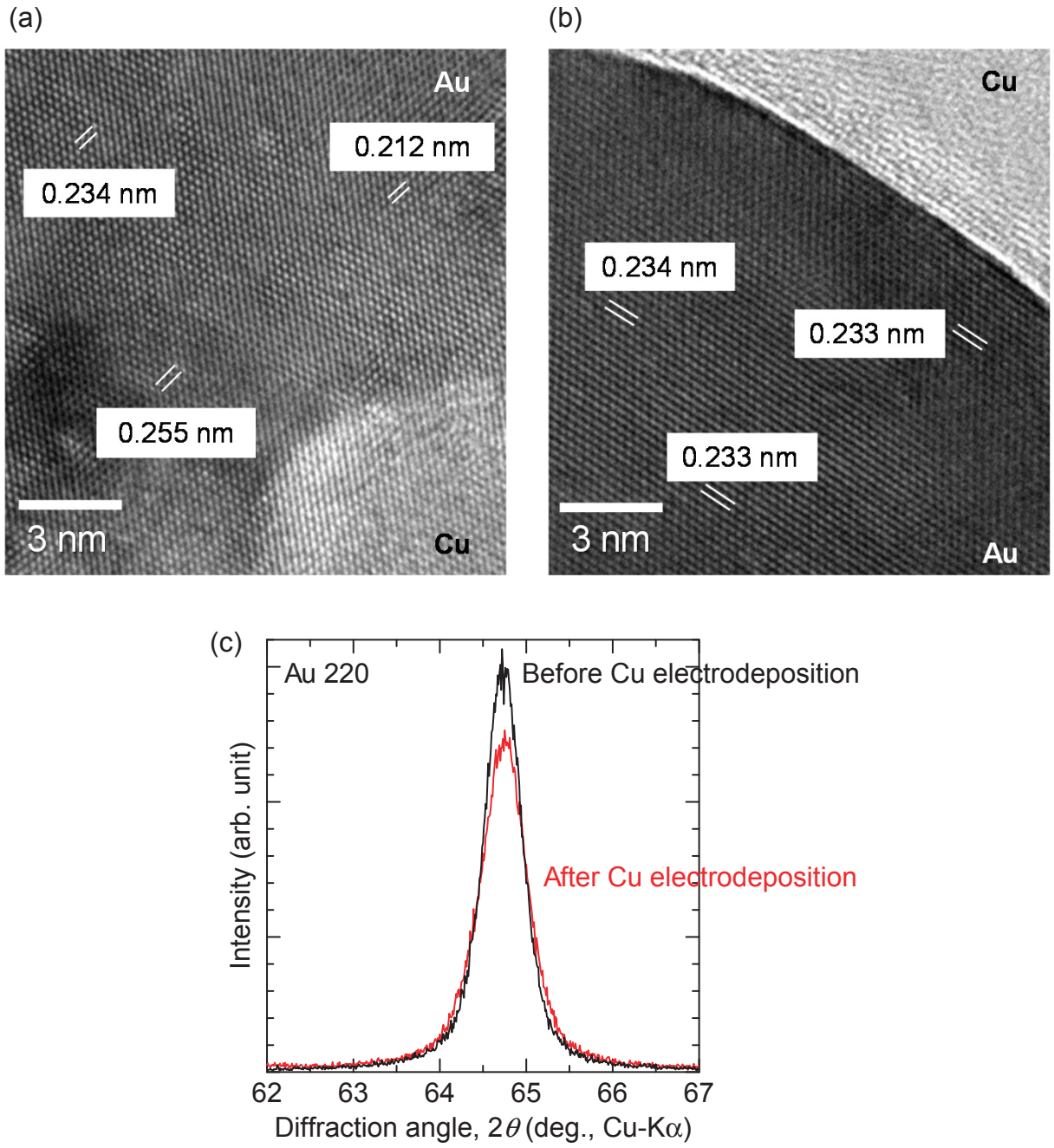

Figure 7

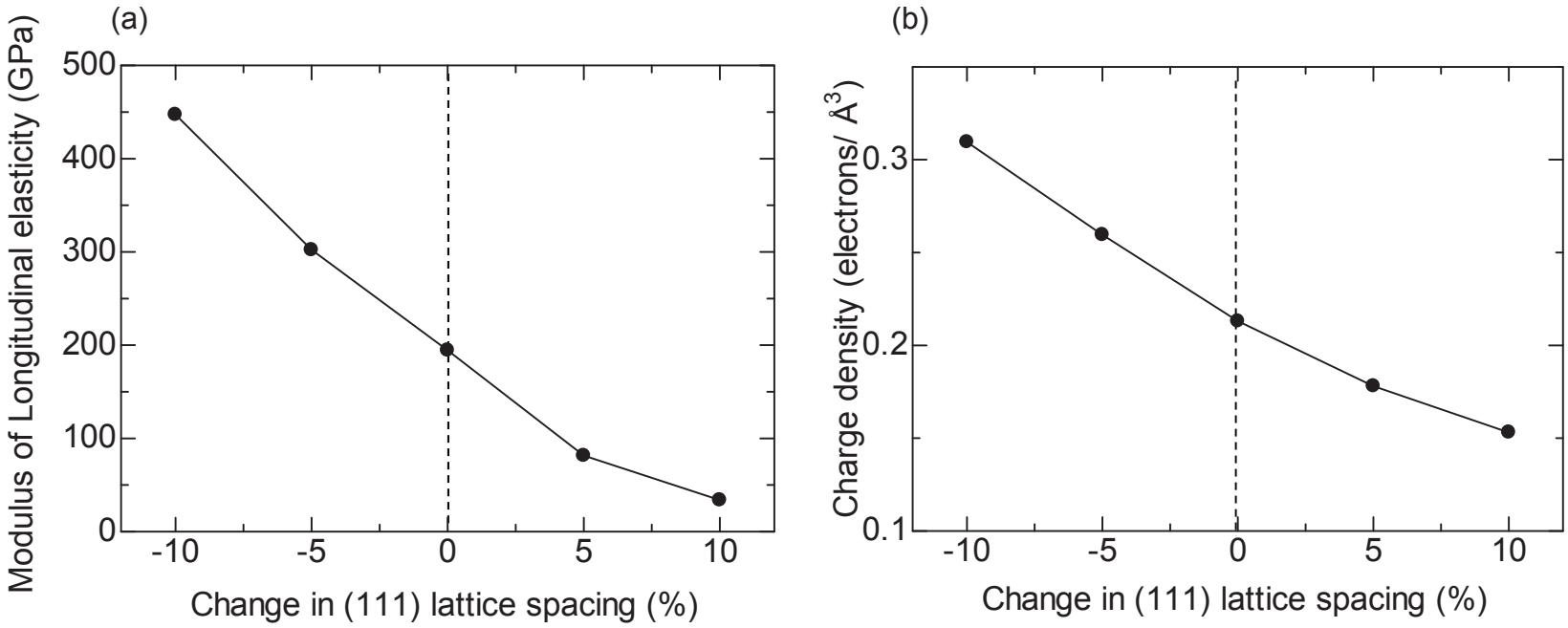

Figure 8